Journal of Hydrology 570 (2019) 726–738

Contents lists available at ScienceDirect

Journal of Hydrology

journal homepage: www.elsevier.com/locate/jhydrol

Streamflow partitioning and transit time distribution in snow-dominated basins as a function of climate

Zhufeng Fang[a,*], Rosemary W.H. Carroll[a,b], Rina Schumer[a], Ciaran Harman[c], Daniel Wilusz[c], Kenneth H. Williams[b,d]

[a] Desert Research Institute, Reno, NV, USA
[b] Rocky Mountain Biological Laboratory, Gothic, CO, USA
[c] Johns Hopkins University, Department of Environmental Health and Engineering, Baltimore, MD, USA
[d] Lawrence Berkeley National Laboratory, Berkeley, CA, USA

ARTICLE INFO

This manuscript was handled by Peter K. Kitanidis, Editor-in-Chief, with the assistance of Vahid Nourani, Associate Editor

Keywords:
East River
Snowmelt
Travel time distributions
Hydrologic model
Warming climate

ABSTRACT

Snowmelt is the principal control on the timing and magnitude of water flow through mountainous watersheds. The effects of precipitation type and quantity on storage and hydrologic connectivity in mountainous systems were explored by combining the observed stable isotope $\delta^{18}O$ in rain, snow, snowmelt, and streamflow with numerically simulated hydrologic boundary fluxes and inverse techniques applied to transient travel time distributions (TTD) using StorAge Selection (SAS) functions. Hydrologic simulations of the East River (ER, 85 km^2), a snow-dominated Colorado River headwater basin, for water years 2006–2017 were used to test a diverse set of snow accumulation scenarios. During the snowmelt period, the ER released younger water during high storage periods across seasonal and annual timescales (an "inverse storage effect"). Additionally, more young water was released from storage during wet years than during dry years. However, wet years also appeared to increase hydrologic connectivity, which simultaneously flushed older water from the basin. During years with reduced snowpack, flow paths were inactivated and snowmelt remained in the subsurface to become older water that was potentially reactivated in subsequent wet years. Incremental warming in hydrologic model simulations was used to evaluate TTD sensitivity to precipitation changing from snow to rain. Despite the altered timing of boundary fluxes because of warming, years with basin average precipitation above 3.25 mm d^{-1} (1200 mm y^{-1}) were resilient to temperature increases up to 10 °C with respect to annual water balance partitioning and streamflow TTD. In contrast, years with less precipitation were sensitive to increased temperatures, showing marked increases in the fraction of inflow lost to evapotranspiration. Younger water was preferentially lost to evapotranspiration, which led to an increase in the mean age of streamflow in drier years.

1. Introduction

The Colorado River is a major water source and economic engine for seven Western states; 90% of its water originates from the snow-dominated upper watersheds of the Rocky Mountains in Colorado, Utah, and Wyoming (Jacobs, 2011). The upper watersheds, like most snow-dominated headwaters around the world, are considered especially vulnerable to climate change. Increased temperatures have significantly affected water budget components at snow-dominated watersheds by reducing the snow precipitation fraction (Foster et al., 2016) and increasing the surface energy budget, which drives more evapotranspiration (*ET*) (Flerchinger et al., 1996). Recently, frameworks have been developed to quantify the response of water budget component partitioning at snow-dominated watersheds. For example, a basin characterization model (BCM) suggests a decrease in runoff and an increase in evapotranspiration with a shift in precipitation from snow to rain (Longley, 2017). A water and energy budget distributed hydrological model with improved snow physics (WEB-DHM-S) suggests a warming climate reduces the contribution of snowmelt to streamflow discharge (Bhatti et al., 2016). However, further frameworks are still needed to quantify not only the water component partitioning, but also when snowmelt and rain reach the snow-dominated system and the travel time to the streamflow outlet.

There are two significant motivations for studying the timing and sufficiency of snowmelt at snow-dominated systems. First, spring snowmelt increases subsurface storage and activates predominantly fast

* Corresponding author at: Division of Hydrologic Sciences, Desert Research Institute, 2215 Raggio Parkway, Reno, NV 89512, USA.
E-mail address: Zhufeng.Fang@dri.edu (Z. Fang).

https://doi.org/10.1016/j.jhydrol.2019.01.029
Received 19 December 2018; Received in revised form 14 January 2019; Accepted 24 January 2019
Available online 29 January 2019
0022-1694/ © 2019 Elsevier B.V. All rights reserved.

flow paths through overland flow and interflow (Heidbüchel et al., 2012) (Webb et al., 2018). Monsoonal events are believed to activate only occasional fast flow paths because summer monsoon rain is largely consumed by *ET* and is not an important streamflow contributor compared with snowmelt (Vivoni et al., 2010). Dry periods in the spring and fall show similar streamflow responses dominated by slow flow paths through the fractured bedrock. Second, snowmelt is the dominant driver of infiltration (Siderius et al., 2013) and plays a key role in chemical transport. For example, NO_3^- and dissolved organic carbon (DOC) export are greater during melt season than in winter with consistent snow cover (Brooks et al., 1998) (Finlay et al., 2006). Greater SO_4^{2-} dilution, smaller discrepancies between HCO_3^- and cation-equivalent concentrations, and smaller CO_2 efflux rates from surface waters occur during spring melt (Winnick et al., 2017). These flow paths and chemical transport dynamics will become more complicated with climate change and temperature increases. Therefore, quantifying variations in the amount and timing of spring snowmelt under different warming scenarios is very important.

Stream water age distribution is a measure of a catchment's memory of past inputs, and therefore it can be used to understand the sensitivity of hydrologic flow and transport processes to climate change. Since the 1960s, isotope hydrograph separation (IHS) techniques have been widely used to study the age and residence time of stream water. Traditional IHS methods rely on two end members and a well-mixed system. However, time and space invariance as well as neglect of soil water contributions in HIS methods have been challenged in recent studies (e.g., Casper et al. (2003) and Klaus and McDonnell (2013)). Advanced IHS methods were recently developed to avoid these problems. For example, Kirchner (2019) proposed an ensemble hydrograph separation based on correlations between tracer fluctuations that assume end-member signatures are time-invariant before and during each storm event.

Another approach that can explicitly account for the mass balance of both water and tracers is the use of travel time distributions (TTD). A TTD represents the distribution of the ages of water parcels exiting a system relative to when they entered as rain or snowmelt. Decoding catchment TTDs has primarily relied on direct observation (Payn et al., 2008), mechanistic modelling and particle tracking (Maxwell, 2013; Sanford and Pope, 2013), and spectral analysis (Kirchner et al., 2000) of stable isotopes such as δ^2H and $\delta^{18}O$ and conservative tracers such as chloride and bromide (McGuire and McDonnell, 2006) via direct observation (Payn et al., 2008), mechanistic modelling and particle tracking (Maxwell, 2013; Sanford and Pope, 2013), and spectral analysis (Kirchner et al., 2000). A traditional TTD estimate often assumes a constant input and output flow rate or a uniform water parcel selection without bias toward any age set (well-mixed tank). There is increasing evidence that age composition is not time invariant, but that water partitions dynamically because of overland flow, hydrologic connectivity, flow paths, and varying velocities. Specifically, rapid transfers of young water will preserve some of the isotopic variability of precipitation in stream outflow, whereas longer flow paths transfer a broader distribution of ages, which significantly dampen the input signal. These processes can be captured by computing time-variable TTDs that incorporate multiple dynamics based on conservation equations for both mass and age (Botter et al., 2011; Van Der Velde et al., 2012; Harman 2015). To solve the conservation equation, a relationship that determines how the distribution of discharge ages is selected from the distribution of stored water ages must be provided. The StorAge Selection (SAS) function captures this relationship. A SAS function must be provided for each outflow, such as stream discharge and *ET*. Variations of this approach include absolute StorAge Selection functions (aSAS) (Botter, 2012; Botter et al., 2011), fractional StorAge Selection functions (fSAS) (van der Velde et al., 2015; Van Der Velde et al., 2012), and rank StorAge Selection functions (rSAS) (Harman, 2015). These theoretical advances have been applied at small-scale rain-dominated watersheds (Benettin et al., 2017; Harman, 2015; Wilusz et al., 2017). However, they have not yet been applied to larger-scale snow-dominated basins, partly because of the challenges of quantifying snow accumulation and melt in topographically complex terrain (Bales et al., 2006; Molotch et al., 2009; López-Moreno et al., 2014; Gustafson et al., 2010) as well as determining snowpack isotopic evolution and its dependence on melt rate (Taylor et al., 2001).

To address the challenges of spatial and temporal variability in high-altitude snow and rain precipitation and quantify stream TTDs, we combined field observations with a multi-model strategy. Specifically, we developed a hydrologic model for water years 2006–2017 to estimate the spatially distributed water budget components of precipitation, snowmelt, discharge, groundwater storage, and *ET*. Simulated hydrologic fluxes were then used to run the SAS model. The SAS function parameters were calibrated to reproduce observed $\delta^{18}O$ in rain, snow, snowmelt, and streamflow, and then used to simulate TTDs. In addition to being the first use of SAS theory for a large-scale snow-dominated watershed, this study connected snow-driven water budget components to streamflow TTDs to assess their sensitivity to inter-annual variations in precipitation and temperature. Using the tools developed, we asked the following questions:

1) How do TTDs vary in response to seasonally variable snowmelt?
2) How do TTDs vary in response to annually variable snowmelt precipitation?
3) How do TTDs vary with temperature increases and the conversion of snow to rain in both wet and dry years?

2. Site description

The study site is the East River (ER, Fig. 1) located in Gothic, Colorado. The ER contributes 20% of streamflow to the Gunnison River, which then contributes 40% of the discharge to the Colorado River at the Colorado-Utah state line (Battaglin et al., 2011; Markstrom et al., 2012). The ER is considered representative of many snow-dominated headwaters in the Rocky Mountains (Markstrom et al., 2012). For a comprehensive description of the ER, see (Carroll et al., 2018). The study catchment is 85 km^2 with a nearly 1.4 km vertical drop in elevation (4120 m to 2760 m) and it contains pristine alpine, subalpine, montane, and riparian ecosystems. The river resides primarily in the Cretaceous marine shale of the Mancos formation, whereas the highest mountains are formed by Cenozoic igneous formations intruding into the Mancos along the western edge of the study domain and into Paleozoic and Mesozoic sedimentary strata along the eastern edge where these strata form steeply dipping beds that expose older units to the surface (Gaskill et al., 1991). The study area is predominantly barren with sparsely vegetated land cover comprised of alpine conditions (26%), conifer forests (45%), aspens (12%), grasslands (10%), shrubs (2%), riparian cover (3%), and other land cover such as developed land and open water (2%). representing the remaining land cover (Ryan and Opperman, 2013).

The ER experiences long, cold winters and short, cool summers. There are two snow-telemetry (SNOTEL) sites in the vicinity of the ER domain (Fig. 1): Schofield (Site Number: 737) and Butte (Site Number: 380) at elevations 3261 m and 3097 m, respectively. Snowfall occurs October through May, and monsoonal rains generally begin in mid-July and last into September. Annual average (± standard deviation) precipitation at Scofield over the period of record is 1200 ± 233 mm yr^{-1}, with 70% ± 8% falling as snow. Butte annual precipitation is nearly half at 670 ± 120 mm yr^{-1}, with snow accounting for 66% ± 12% annual precipitation. Mean daily air temperatures at Butte range from −8.3 °C in December to 11 °C in June, and 1.6 ± 1.2 °C cooler than temperatures at the higher elevation Schofield station. Snowmelt processes dominated the observed discharge exiting the basin (gauge location provided in Fig. 1), with peak flows occurring in early to mid-June. After peak discharge, flow recedes through the summer and fall, and monsoonal storm events occur in late

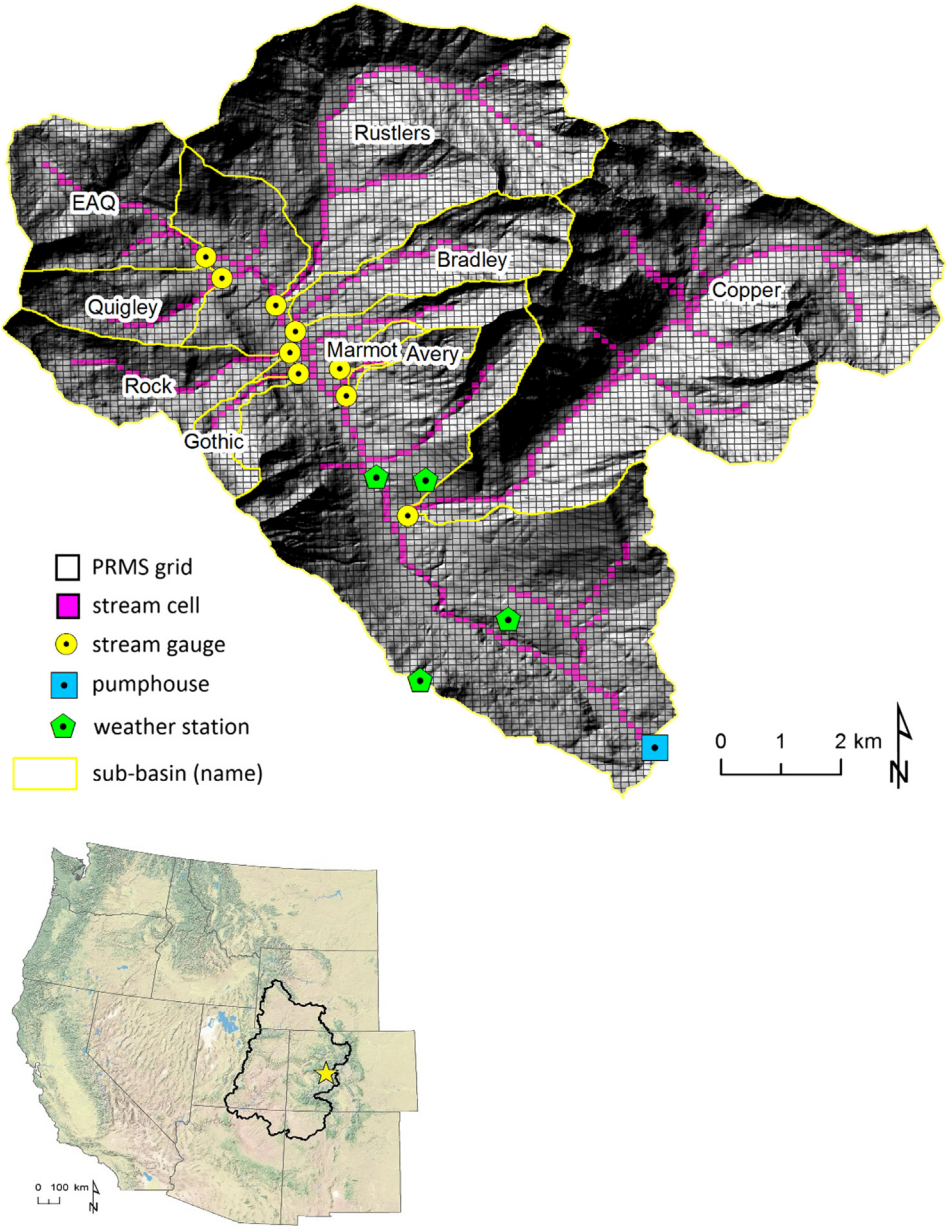

Fig. 1. ER domain with sampling locations identified. (Inset) Location of ER (yellow star) within the western United States and the Upper Colorado River Basin (black outline). (For interpretation of the references to colour in this figure legend, the reader is referred to the web version of this article.)

summer that cause small, transient increases in discharge. Baseflow occurs in the fall and winter months.

3. Methods

3.1. Solute collection and analysis

Collection and analysis of rain, snow, snowmelt, and streamflow for $\delta^{18}O$ (ratio of stable isotopes oxygen-18, in Vienna Standard Mean Ocean Water [VSMOW] standard) analysis (sites provided in Fig. 1) are described by Carroll et al. (2018) and provided here in brief. All samples were filtered at (Pall, NY, USA; PTFE; 0.45 μm) and were placed in 1.5 mL glass vials with Teflon™-coated septa lids. Rain ($n = 70$) and snow ($n = 89$) grab samples were collected at a single location from July 2014 to October 2017. In addition, weekly aggregated rain samples ($n = 46$) were collected to assess spatial variability in precipitation at four locations (Fig. 1). The rain gauges used in this study are described by Carroll et al. (2018). Snowmelt was collected *in situ* during 2016 and 2017. Fig. 1 shows four snowmelt locations. Collection devices were modified in 2016 and updated in 2017 to include a 56 cm × 66 cm × 10 cm polyethylene tray and 2 cm diameter bulkhead to drain snowmelt into a 5L buried reservoir. Melt collection using a peristaltic pump began April 1, 2014 and continued weekly until full melt was achieved ($n = 56$). Stream water samples were collected daily from May 1, 2014, to September 30, 2017, using an automatic water sampler (Model 3700; Teledyne ISCO, NE, USA) via a peristaltic pump and uncapped 1 L polyethylene bottles. Each bottle was filled with 2 cm of mineral oil to eliminate evaporation effects between the collection and retrieval of samples. The oxygen isotope ratios of the water samples were measured using an off-axis integrated cavity output spectrometer coupled with an auto-sampler interfaced with a heated injector block (Los Gatos Research, San Jose, USA). Isotope ratios are reported in conventional δ-notation relative to the Vienna Standard Mean Ocean Water scale. Repeated measurements of laboratory standards associated with sample analysis yielded $\delta^{18}O$ of $-11.44 \pm 0.18‰$ (1σ).

3.2. Stream discharge

Stream discharge was measured at the pump house (PH, gauge location provided in Fig. 1) for water years 2015 to 2017. Instantaneous readings were measured using a SonTek Flow Tracker® acoustic Doppler velocimeter to create a depth-discharge relationship in conjunction with Solinst Levelogger Edge® pressure transducers corrected with barometric pressure. Correlating daily flows with the United States Geological Survey (USGS) East River at Almont (09112500) stream gauge, located approximately 25 km downstream from the study site, allowed stream discharge to be corrected during periods of winter ice when pressure transducer readings can be anomalously high and stream discharge estimates to be extended prior to observation.

3.3. Hydrologic numerical model

Hydrologic analysis of the ER was done using the USGS Precipitation-Runoff Modelling System (PRMS) (Markstrom et al., 2015) to account for flow within and between the plant canopy and soil zone, streams, and the groundwater system. Climate data drive PRMS calculations to spatially distribute the precipitation amount and type, solar radiation, potential *ET* (*PET*), sublimation, canopy interception, soil evaporation and transpiration, snowmelt, infiltration, recharge, and groundwater storage. Supplemental information (SI) provides detailed information on the PRMS framework, parameterization, calibration, and simulated water budgets. The model grid resolution is 100 m and simulations are run at the daily time step for water years 2006 to 2017 (from October 1 to September 30) to capture a range of snow accumulation scenarios. The PRMS parameters of dominant cover type, summer and winter cover density, canopy interception characteristics for snow and rain, and transmission coefficients for shortwave radiation provided in Fig. S.9 were derived using the USGS Landfire vegetation maps (Ryan and Opperman, 2013). Climate inputs of daily minimum and maximum temperature were obtained from the two local SNOTEL stations and spatially distributed as a function of daily lapse rate between stations, with additional adjustment for cell aspect. Daily precipitation measured at the Butte SNOTEL was spatially distributed across the watershed using the Parameter-elevation Regression on Independent Slopes Model mean monthly precipitation patterns for water years 1981 to 2010 (Daly et al., 2008).

The model was calibrated to match the precipitation type at the Butte SNOTEL, the monthly average solar radiation observed at four weather stations located in the ER (Fig. 1), and the observed streamflow at the PH site and several upstream gauge locations to ensure the spatial origin of streamflow was representative (Fig. S.12). The sensitivity of hydrologic partitioning to changing temperatures and associated shifts in precipitation type from snow to rain was tested by incrementally increasing minimum and maximum daily temperatures from 2 °C to 15 °C above historically observed values. The PRMS-simulated daily effective precipitation (P_{eff} = snowmelt + rain), soil *ET*, groundwater storage, and stream discharge were used in conjunction with observed δ^2O (described in Section 4.2) to define the isotopic mass flux needed for TTD development.

3.4. Isotopic mass flux

Fig. 2 shows the observed seasonal variation in isotopic signature in rain, snow, and snowmelt for May 1, 2014, to September 30, 2017. Grab samples of rain were at maximum depletion in January (snow) and minimum depletion in August (rain). On average, $\delta^{18}O$ in the snow grab samples was −17.8 ± 5.8‰, whereas it was −8.3 ± 4.3‰ in the rain grab samples. The weekly aggregated rain samples collected at locations across the basin, which varied greatly in elevation, exhibited isotopic values that were similar to the rain grab samples but with less variability. Snowmelt samples collected in the spring of 2016 and 2017 were depleted compared with the snow grab samples because

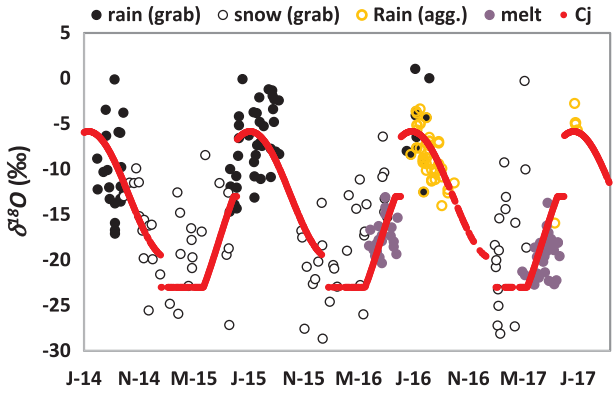

Fig. 2. Observed $\delta^{18}O$ in rain, snow, and snowmelt with estimated C_j for SAS input. Agg. = weekly aggregated.

enrichment occurred over the melt period. Observed stream discharge $\delta^{18}O$ ranges from −12.28‰ to −17.97‰. Generally, $\delta^{18}O$ declines throughout the winter months and reaches its annual minimum during spring melt, after which it rebounds toward the annual maximum in the late summer and fall.

Sinusoidal functions were developed following previous studies (e.g., Allen et al., 2018; Stockinger et al., 2017) to smooth observed data for SAS input and allow extrapolation of precipitation mass for the entire PRMS simulation. Functions minimized the root-mean-square error in observed values. The fitting equations for rain and snowmelt are:

$$\delta^{18}O = 7sin\left(0.172x + \frac{170\pi}{180}\right) - 12.85 \quad (1)$$

$$\delta^{18}O = 9sin\left(0.172x + \frac{150\pi}{180}\right) - 18 \quad (2)$$

where x = water year day. Snowmelt values were truncated to the observed minimum (-13‰) and maximum (−23‰) values to limit unreasonable values, especially with potential melt in the winter. The two sine functions were combined for a single SAS input function representing C_j. During the period when basin-wide Snow Water Equivalent (*SWE*) was ≥0.3 (the maximum *SWE* for a given year), the snowmelt function was used. When *SWE* < 0.3, the basin was predominantly snow free, and therefore the rain function was used. The resulting mass inflow was calculated as $-P_{eff} \times C_j$ such that heavily depleted values during rapid snowmelt were expressed as large positive mass flux (Fig. 3). For example, 2017 was a wet year with large melt rates that drove a large mass influx of $\delta^{18}O$, and therefore stream discharge responded with a more depleted $\delta^{18}O$ signature.

3.5. SAS theoretical considerations and inverse model approach

We chose to use a method in which the SAS function related the TTD to age ranked storage rather than absolute age (Harman, 2015). This

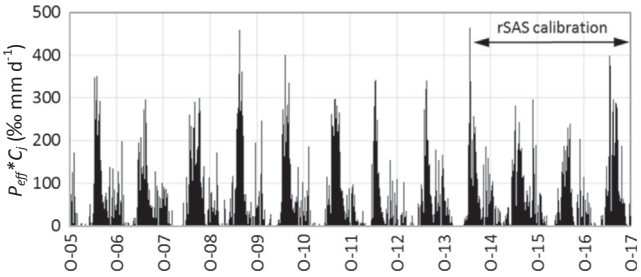

Fig. 3. Mass inflow of $\delta^{18}O$ over the simulation period from 2006 to 2017 for historical conditions. The SAS calibration period is marked for reference.

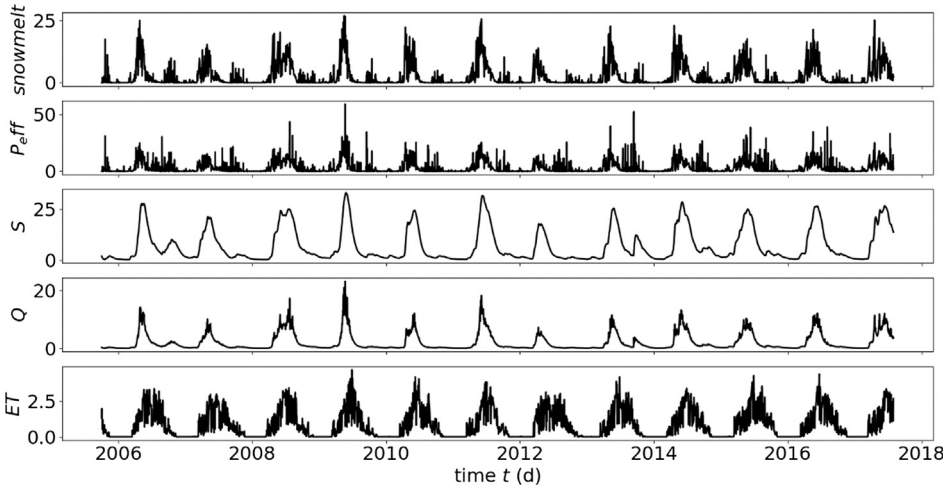

Fig. 4. PRMS simulated water balance components for water years 2006 to 2017. Units of evapotranspiration (*ET*), discharge (*Q*), effective precipitation (P_{eff}), and snowmelt are normalized by basin area to equal to mm d^{-1}. Unit of groundwater storage (*S*) is mm.

method did not contain *a priori* conceptual assumptions that partition the watershed into a number of compartments. Instead, a functional form for the SAS function was assumed, and its parameters were calibrated using stable isotope observations. Theoretical considerations provided by others (Harman, 2015; Rinaldo et al., 2015) are provided here in brief. The backward cumulative TTD of outflows represents the distribution of water parcels at age T or younger that are leaving the system as discharge $\overleftarrow{P}_Q(T, t)$ or evapotranspiration $\overleftarrow{P}_{ET}(T, t)$ at time *t*. In a hydrologic system with a total storage *S(t)*, the continuity of water age and mass can be expressed as:

$$\frac{\partial S_T(T,t)}{\partial t} = J(t) - Q(t)\overleftarrow{P}_Q(T,t) - ET(t)\overleftarrow{P}_{ET}(T,t) - \frac{\partial S_T(T,t)}{\partial T} \tag{3}$$

where $J(t)$, $Q(t)$, and $ET(t)$ are inflow, discharge, and *ET* at time *t*, respectively. The latter three terms on the right-hand side of Eq. (3) represent parcels with age at or younger than T that either leave the system as discharge or evapotranspiration, or become older than age T during Δt. The age-ranked storage, $S_T(T, t)$, is related to the residence time distribution ($P_S(T, t)$, which is the fraction of storage at time t with an age less than T that can be expressed as:

$$S_T(T,t) = S(t)P_S(T,t) \tag{4}$$

Eq. (3) is underdetermined and requires additional assumptions to solve. Two SAS functions are used to reexpress $\overleftarrow{P}_Q(T, t)$ and $\overleftarrow{P}_{ET}(T, t)$ as the equivalent CDF of $S_T(T, t)$ instead of T:

$$\Omega_Q(S_T,t) = \overleftarrow{P}_Q(T,t) \tag{5}$$

$$\Omega_{ET}(S_T,t) = \overleftarrow{P}_{ET}(T,t) \tag{6}$$

For *ET*, we assume a time-invariant uniform distribution for SAS using a single parameter, S_{ET}, to represent a threshold volume of the young water in storage:

$$\Omega_{ET}(S_T) = \begin{cases} \frac{S_T}{S_{ET}} & S_T \le S_{ET} \\ 1 & S_T > S_{ET} \end{cases} \tag{7}$$

We define the SAS function for Q as a time-variant storage-dependent gamma distribution:

$$\Omega_Q(S_T,t) = \frac{\gamma\left(\alpha, \frac{S_T}{\lambda(S(t)-S_c)}\right)}{\Gamma(\alpha)} \tag{8}$$

where γ is the incomplete gamma function, Γ is the gamma function, α is the shape parameter, and λ and S_c relate the scale parameter to the estimate storage. The parameters α, λ, S_{ET}, and S_c are obtained by inverse calibration against observed $\delta^{18}O$ based on the continuity equation of tracer concentration:

$$C_Q(t) = \int_0^\infty C_J(t-\tau)\overleftarrow{p}_Q(\tau,t)d\tau \tag{9}$$

where C_J and C_Q are the tracer concentration of inflow and outflow, respectively, and $\overleftarrow{p}_Q$ is the PDF of $\overleftarrow{P}_Q(T, t)$. Eqs. (3) and (4) are solved using Eqs. (5) through (8) to get the time-variant backward TTD at the outflow and the corresponding fraction of water given age ≤ T.

Parameter ESTimation (PEST) is a general-purpose, model-independent parameter estimation and model predictive uncertainty analysis package that uses parallel programming to boost optimization efficiency (Doherty, 2015). The PEST optimization was done by adjusting α, λ, S_{ET}, and S_c to best match observed $\delta^{18}O$ in stream discharge for water years 2015 to 2017. Hydrologically, this three-year calibration period covers a low, medium, and high snow accumulation period. The PEST-calibrated SAS was then applied to the PRMS simulated boundary fluxes for water years 2006 to 2017 to address precipitation and temperature controls on streamflow age distributions. Similar to the test conducted for hydrologic partitioning, the sensitivity of streamflow TTD to changing temperatures and associated shifts in precipitation type from snow to rain was tested by incrementally increasing temperatures from 2 °C to 15 °C above historically observed values. This scenario study provided insight into how stream TTD in wet and dry years responded differently to climate change.

4. Results

4.1. Simulated water budget

Water budget components P_{eff}, *ET*, groundwater storage (*S*), and stream discharge (*Q*) at the Pumphouse (PH) site were derived using the PRMS model (Fig. 4). Over the 12-year simulation period, P_{eff} was highest in 2011 (mean P_{eff} = 4.06 mm d^{-1}) and lowest in 2012 (mean P_{eff} = 1.98 mm d^{-1}), which represent typical wet and dry conditions, respectively. In this study, streamflow was simulated to be the combined surface runoff, interflow, and groundwater. Total *ET* was broken into the components of soil *ET* (ET_s), sublimation, and canopy evaporation. The SAS model used the basin-averaged PRMS-simulated daily values of P_{eff}, ET_s, *S*, and *Q* (Eqs. (3) to (9)) to estimate TTDs variations under different climate situations. Refer to Supplemental Information Sections (SI) S.2.4 and S.3 for further discussion about water budget component variations and their responses to temperature increases.

The East River watershed hydrology is dominated by snow

accumulation and melt. In general, this headwater basin is not water limited and *ET* is fairly uniform over the historical range in precipitation. We found that the other water budget components —such as P_{eff}, Q, and groundwater storage, as well as snowmelt percentage (sm %)—vary from wet years to dry years. In warmer years (both wet and dry), effective precipitation is more evenly distributed over time, as opposed to the pulse input during spring melt that occurs in colder years (see Figs. S.18 through S.20). This is because in warmer years, winter rain frequency is greater and earlier spring snowmelt occurs, which leads to earlier increases of recharge, storage, and discharge. Previous studies found a similar phenomenon using the basin characterization model (BCM) (Longley, 2017) and global circulation models (GCMs) (Stone et al., 2002). However, the total discharge, recharge, and groundwater storage declined sharply in spring and summer. Such a decline was also found in a Parflow-CLM study (Gilbert and Maxwell, 2018), GCMs (Zhai et al., 2017), and WEB-DHM-S model (Bhatti et al., 2016). The new findings from this study were that during wet years, such as 2011, water in excess of system *ET* buffered hydrologic response to climate variability and, despite large seasonal changes in snowmelt amount and timing, the annual partitioning of P_{eff} into stream discharge, soil *ET*, soil moisture, *fGW*, and subsurface storage only changed slightly with temperature increases < 7 °C (Fig. S.19). Only during extreme warming (temperature increases of 10 °C to 15 °C) did the basin respond hydrologically at the annual scale through significant increases in *ET* and subsequent decreases in streamflow. In contrast, dry years showed hydrologic sensitivity at much lower temperature increases (Fig. S.20). Evapotranspiration increased sharply at the expense of streamflow (Fig. S.18cd). This finding highlights the significant effect of warming on extending droughts at high-altitude snow-dominated basins (Barnett et al., 2005; Diffenbaugh et al., 2013).

4.2. Stream discharge TTD as a function of hydrology

Table 1 lists the PEST optimization of SAS parameters α, λ, S_{ET}, and S_c and their uncertainty ranges with simulated stream $\delta^{18}O$ concentrations (C_j) (provided in Fig. 5). The predicted C_j agreed well with the observed values during winter and spring snowmelt season, but it was consistently overestimated for the summer monsoon season, which starts in early July.

We defined four categories of water based on age: very young water (T < 50 d), young water (leaves the system in the same water year as it enters, referred to as T < 1 y), old water (leaves the system in the next 1 to 5 years, referred to as 1 < T < 5 y water), and very old water (stays in the system more than 5 years, referred to as T > 5 y water).

We first focused on the effect of melt water on TTDs at a seasonal timescale. Fig. 6 compares seasonal variations in cumulative TTDs and 95% confidence limits with the representative wet year 2011 and dry year 2012. Winter, or pre-melt, occurs from December to early March, when snowmelt rates are < 1 mm d^{-1} (dashed curves). Spring melt occurs from mid-March to mid-June, when snowmelt rates exceed 8 mm d^{-1} (solid curves). Spring snowmelt drives streamflow TTD toward a greater younger water fraction than during pre-snowmelt. Approximately 24% of the very young water (T < 50 d) flowed out of the system during the spring melt season, whereas the winter season experienced a sharp increase in P_Q, which is indicative of older water. The daily correlation between the fraction of T < 50 days and snowmelt (r = 0.64, $p \ll 0.01$) stresses the importance of snowmelt on the mobilization of very young water, and the positive and significant correlation to groundwater storage (r = 0.77, $p \ll 0.01$) highlights the movement of young water from the basin when groundwater storage is high. A recent study (Webb et al., 2018) found that hydrologic connectivity increased slowly with the accumulation of introduced precipitation, and then it reached a threshold where deep flow paths were activated and the previously immobilized water was quickly transported to the system outlet. Our SAS-model-simulated TTDs provided insight into the variation of the hydrologic connectivity during the melt and pre-melt seasons. In spring, flow paths become active almost immediately with the entry of abundant snowmelt and consequent increase in groundwater storage, and more young water leaves the system quickly via active flow paths. However, in winter, limited introduced precipitation leads to inactivated deep flow paths, and therefore more young water is immobilized in deep zone. Similarly, a previous study linking detailed oxygen 18 observations of stream water, melt water, soil water, and groundwater with hydrometric measurements in a small catchment in northern Sweden during the snowmelt period demonstrated this complementary deep flow path activation when a high amount of event snowmelt water infiltrated into the system in spring (Laudon et al., 2004).

Table 1
SAS optimized parameters and 95% confidence limits.

Parameter	α	λ	S_{ET} (mm)	S_c (mm)
Optimized value	0.225	−200.95	18.65	2047.74
Uncertainty range	[0.217, 0.234]	[-554.74, −152.84]	[7.87, 44.23]	[376.39, 11140.60]

At annual timescales for the entire simulation period from 2006 to 2017, the correlation coefficient ($r_{YWF-Peff}$) for the very young water fraction (YWF, T < 50 d) increased during years with larger snow accumulation and larger inflow P_{eff} rates. For example, r = 0.71 in 2011 and r = 0.44 in 2012. The direct relationship between P_{eff} and the YWF correlation coefficient $r_{YWF-Peff}$ is significant (r = 0.84, $p \ll 0.01$) because it further suggests that young water mobilization is a function of wet conditions and that there is less young water mobilization under dry conditions.

Fig. 7 illustrates the relationship between young water (T < 1 y) and old water (T = 1–5 y) based on the inflow and outflow distributions that contribute to streamflow as a function of P_{eff}. The P_{eff} for the inflow year is defined by the year it enters the watershed, whereas the P_{eff} for the outflow year refers to the P_{eff} related to the year of discharge. At the annual scale of analysis, inflow year and outflow year are equivalent for T < 1 y. For old water (T = 1–5 y), we investigated two cases. For the first case, we investigated how much of the water that entered the system for a given year (e.g., year 2011) left the system in 1 to 5 years as old water. For the second, we investigated how much old water that entered the system in the previous 1 to 5 years left the system in a given year (e.g., year 2011). The results of first case indicated that young water (T < 1 y) was highly dependent on the amount of precipitation (r = 0.86, slope = 0.20, $p \ll 0.01$, Fig. 7 circle marker). The amount of old water (T = 1–5 y) leaving the system was also dependent on the magnitude of P_{eff} for the year that water entered the system, but with a lower slope and lower significance (r = 0.49, slope = 0.08, p < 0.01, Fig. 7 cross markers) than T < 1 y. Table 2 provides the amount of water in a given inflow year that leaves in future years. For example, in 2011, inflow P_{eff} = 4.06 mm d^{-1} and Q = 2.85 mm d^{-1}. The amount of water with age T < 1 in 2011 was 0.70 mm d^{-1}, or 17% inflow P_{eff} and 25% of total stream discharge for that year. Water that entered the basin in 2011 that left 1 to 5 years later was 0.39 mm d^{-1}, or 10% of 2011 inflows, whereas 73% of inflowing P_{eff} stayed in the basin longer than 5 years. During 2012, a representative dry year, P_{eff} = 1.98 mm d^{-1} and streamflow was 1.41 mm d^{-1}. Water transported to the stream in < 1 year was 0.27 mm d^{-1}. This is less than half the volume of young water leaving in a wet year, which accounts for a lower fraction of 2012 inflow P_{eff} (13%) and of total stream discharge (19%) compared with 2011. Water that entered the basin in a dry year and left in 1 to 5 years was also less than that transported during a wet year, summing to 0.16 mm d^{-1}, or only 8% the inflow volume of 2012.

The different transport ability in wet and dry years can also be explained by the hydrologic connectivity theory: high annual P_{eff} input keeps deep flow paths active to release more water to discharge. In contrast, dry years with low P_{eff} lose a larger component of inflow to *ET*,

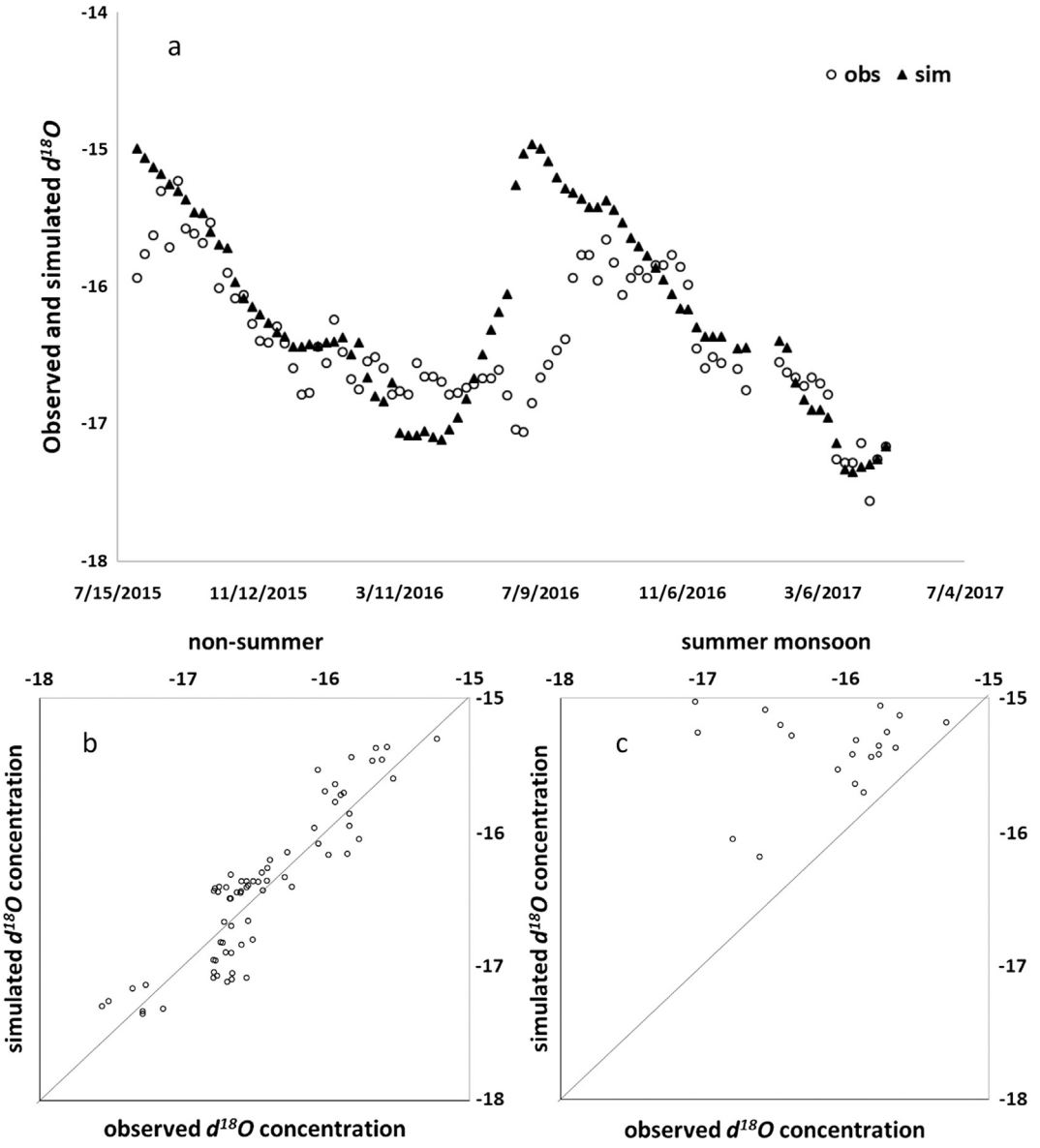

Fig. 5. Comparison of observed and simulated $\delta^{18}O$ in stream discharge from 2015 to 2017 (a) with scatter plots of observed and simulated $\delta^{18}O$ concentration in non-summer season (b) and summer monsoon season (c).

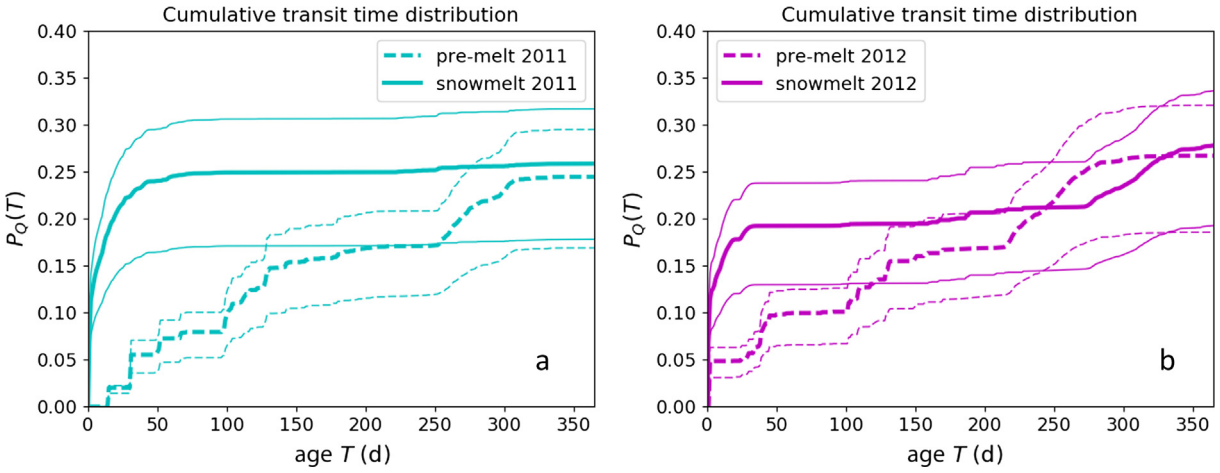

Fig. 6. Seasonal variability in $P_Q(T)$ between a representative (a) wet and (b) dry year; 95% confidence limits delineated.

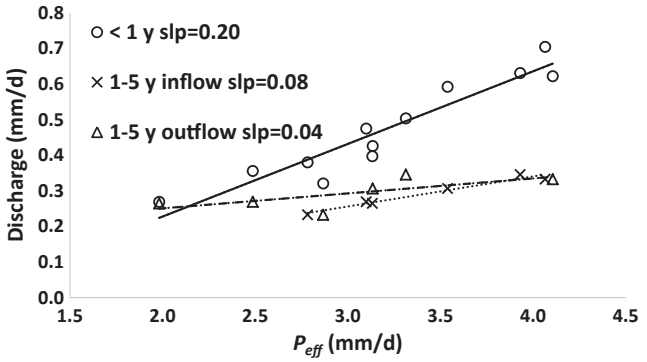

Fig. 7. Magnitude of discharge by age class as a function of mean annual P_{eff} of inflow year and outflow year. Note that for $T < 1$ y, P_{eff} assigned to inflow and outflow year are equal.

leading to declines in groundwater storage and decreases in hydrologic connectivity. Subsequently, less young water is flushed to the stream and more water remains in storage, or moves slowly through the subsurface to be flushed in subsequent years. We noticed that young water in discharge is more sensitive (slope = 0.20, circle markers) to change in P_{eff} than old water (slope = 0.08, triangle markers), indicating that the system prefers to release younger water with P_{eff} increases. Previous studies applying the SAS approach on rain-dominated hydrologic systems suggested the inverse storage effect, in which watershed systems release predominantly younger water to stream discharge when groundwater storage is high or precipitation events are large (Benettin et al., 2017; Harman, 2015; Wilusz et al., 2017). This phenomenon also appears to occur in snow-dominated watersheds at both seasonal and annual timescales.

In the second case, water originating from 1 to 5 years prior to 2011 and leaving as stream discharge in 2011 summed to 0.39 mm d^{-1}, or 14% total stream discharge (Table 2). The remaining 61% of 2011 streamflow by volume older than 5 years was not captured by the model simulation period. Water originating 1 to 5 years prior to 2012 and released in 2012 as stream discharge was 0.14 mm d^{-1}. This is less than half the magnitude of older water mobilized during a wet year and accounts for 10% of stream volume, which is also less than a wet year. We found that a given year's P_{eff} had better correlation to old water entering the system in the past 1 to 5 years and leaving the system within this given year ($r = 0.96$, Fig. 7 triangle markers) than to the water entering the system this given year that contributed to future 1 to 5 years outflow ($r = 0.49$, Fig. 7 cross markers). This indicates that the fraction of old water in the discharge depends more on the sufficiency of P_{eff} in the year when it leaves the system than in the year when it enters the system.

A recent study applying ensemble hydrograph separation (Kirchner, 2018) supports our conclusion that young water fraction increases with precipitation sufficiency. Interestingly, a previous study using a theoretical framework to estimate TTD (Heidbüchel et al., 2012) showed different results. In the study of (Heidbüchel et al., 2012), estimated TTD using the same isotope, $\delta^{18}O$, at two catchments with different precipitation sufficiencies (one humid and one semiarid). Their results indicated that the wet catchment had less young water ($T < 315$ d) leaving the system and more old water ($T > 315$ d) leaving the system than the dry catchment. This contradicts our conclusion. Further study at the East River basin using the SAS model with spatial variations in precipitation will give us better insight into the spatiotemporal variations of TTD estimates.

We observed stream releases of approximately 20% to 25% of P_{eff} water as discharge in the first 50 days (Fig. 6) and 40% of P_{eff} in 10 years. This fraction is much lower than previous studies that used SAS approaches in which over 40% very young water fraction in the discharge and 80% to 90% of inflow water left the systems in 10 years (Benettin et al., 2017; Harman, 2015; Wilusz et al., 2017). One reason for this lower fraction for precipitation to become discharge is the size of system. All the previous studies were conducted at small-scale watersheds (0.9 ~ 3.5 km^2). Similarly, previous work on the activation of temporary flow paths (Laudon et al., 2004) and variations in hydrologic connectivity (Yang and Chu, 2013) were also conducted at small-scale watersheds. However, this study was conducted at a much larger-scale watershed (85 km^2), where long and tortuous flow paths are likely to extend the transit time for inflow water to reach the outlet. Another reason is that unlike previous studies at rain-dominated systems, our study was conducted at a snow-dominated system. Therefore, the P_{eff} occurs primarily during snowmelt from mid-March to mid-June. Although we treat October 1 as the start of a water year, the melt water actually only has less than half a year to leave the system as discharge to be considered young water (i.e., it leaves the system in the same year). Rainwater infiltration between October and March at rain-dominated watersheds is quickly transmitted to the stream outlet, and therefore it has much more time to leave the system as discharge to be considered young water. The melt water will lose a much higher fraction to *ET* in the following summer season than the rainwater, which travels in the system uniformly through the year, which further decreases the fraction of melt water that leaves the system as discharge.

4.3. Stream discharge TTD as a function of climate

This is the first application of the SAS approach to a watershed-scale, snow-dominated system. We found that streamflow TTDs respond differently to temperature increases between wet years and dry years. We tested different scenarios by increasing the temperature 1, 2, 4, 5, 6, 7, 8, 9, 10, 11, 12, and 15 °C to investigate the response of stream TTD. Fig. 8a shows the changes in fractions of inflow leaving the system with a water age of less than one year. During wet years, changes in streamflow TTDs were buffered from temperature increases. Therefore

Table 2
Average amount of each year's inflow (mm d^{-1}) that leaves the basin in subsequent years, or outflow year.

2006	2007	2008	2009	2010	Water 2011	OUT 2012	Year 2013	2014	2015	2016	2017	mm/d	
0.3973	0.1215	0.0833	0.0534	0.0347	0.0389	0.0172	0.0164	0.0229	0.0181	0.0144	0.0205	2006	
	0.3801	0.1322	0.0587	0.0353	0.0381	0.0165	0.0156	0.0214	0.0167	0.0132	0.0186	2007	
		0.6309	0.1722	0.0730	0.0726	0.0301	0.0278	0.0374	0.0288	0.0224	0.0314	2008	
			0.5925	0.1375	0.0938	0.0356	0.0315	0.0408	0.0305	0.0233	0.0321	2009	**Water**
				0.4749	0.1463	0.0409	0.0338	0.0412	0.0296	0.0222	0.0299	2010	
					0.7044	0.1414	0.0782	0.0817	0.0543	0.0388	0.0508	2011	**IN**
						0.2691	0.0614	0.0400	0.0237	0.0161	0.0203	2012	
							0.3207	0.1422	0.0580	0.0366	0.0439	2013	**Year**
								0.5038	0.1409	0.0599	0.0646	2014	
									0.4259	0.1179	0.0821	2015	
										0.3559	0.1219	2016	
											0.6221	2017	

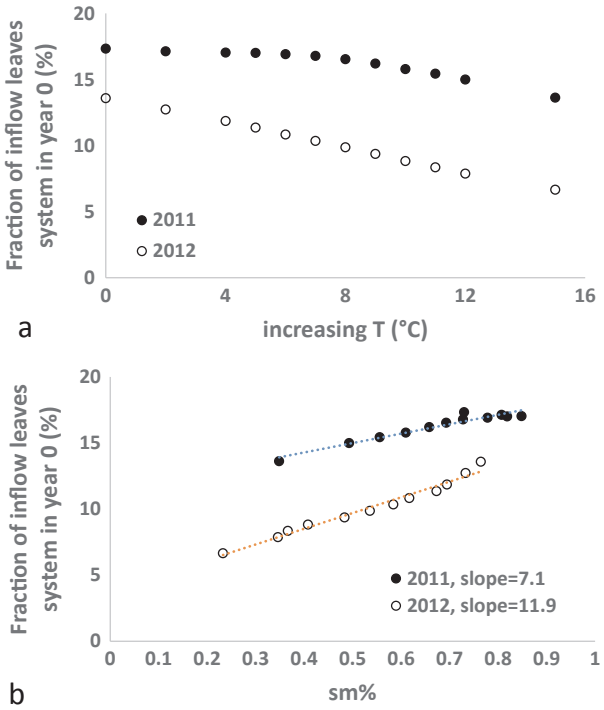

Fig. 8. Implications on warming (a) and snowmelt percentage (sm%) (b) on $T < 1$ y in a wet and dry year.

the amount and fraction of young water released to discharge remained almost unchanged when temperature was increased up to 8 °C. This was because of a sufficient amount of P_{eff} to offset the increasing ET loss due to temperature increases. The amount of young water discharge was not appreciably changed. However, in the case of extreme temperature (increasing by 15 °C), the young water fraction also declined by approximately 14% over the 10 °C case. This was because the sharply increasing ET consumption due to extreme temperature increases exceeded the amount the P_{eff} can afford, and therefore part of discharge was diminished to compensate extensive ET loss.

In contrast, stream discharge TTDs under dry conditions are more sensitive to increased temperatures. A 2 °C increase in temperature reduced the fraction of inflow reaching the river in one year by 5% and a 15 °C increase in temperature reduced young water in the streamflow by 46%. With limited P_{eff}, ET increases diminished stream discharge. Lost groundwater storage offset some of the estimated reductions in streamflow, but the added ET losses resulted in a loss of younger discharge with $T < 1$ y, even with modest changes in temperature. With more significant increases in temperature (i.e., 10 °C), a larger fraction of infiltration was immobilized below the root zone. With temperature increases, the young water fraction in streamflow dropped nearly linearly as a function of the decline in the percentage of snowmelt in P_{eff} (sm%) (Fig. 8b). We found that the slope of a dry year was much higher than a wet year (11.9 to 7.1), indicating that hydrologic partitioning during dry years is more sensitive to increasing temperature and the associated shift in precipitation type.

Fig. 9 shows the fraction of inflow exiting the system in future years given no change and a 10 °C increase in temperature over historical conditions. Wet years see little change in the fraction of inflow P_{eff} leaving the system in future years when temperature increases by 10 °C, whereas dry years experience a significant reduction in the first year, as well as a reduction in the fraction of water leaving the basin over the next 5 years. Water remaining in the subsurface more than 5 years undergoes no obvious change in P_{eff} leaving the system. Despite an increased water limitation ($ET/PET < 1$, refer to SI), dry years result in larger ET loss to warming than wet years (Fig. 9), with loses primarily at the expense of younger water ($T < 1$ y) and to a lesser degree at the expense of old water (T = 1–5 y) to effectively increase the mean residence time of water in the basin.

With increasing temperatures (up to 10 °C), streamflow ages increased for a dry year but remained relatively unchanged for a wet year. For the old water that entered system 1 to 5 years before the wet/dry years, we found that increasing temperature reduces the fraction of the inflow from previous years in the discharge and forces the water to stay longer in the system, which leads more water to be lost as ET. Fig. 10 shows that a rise in temperature has little effect on streamflow age distributions in a wet year, but will delay water leaving the system by more than 30 to 50 days or even longer in a dry year. Such a delay repeats in each dry year and accumulates to cause more old water to either stay in the system over a longer period or to be lost as ET. When temperatures were increased by 15 °C, streamflow $T < 1$ y in a wet year was larger than with no warming in a dry year (Fig. 8a). However, both wet and dry years showed declines in ages $T < 5$ y and age distributions of streamflow increased relative to historical conditions (Fig. 9).

When the majority of P_{eff} shifted from snow to rain with extreme temperature increases beyond 10 °C, P_{eff} was delivered uniformly into the system as rain over the winter and spring, as opposed a pulse of melt only in the spring, which caused the water to reside in the system over a longer period, especially in the dry years (Fig. 10). Subsequently, the temporary activation of deep flow paths by spring melt no longer exists, making the overall hydrologic connectivity decline and the fraction of young water ($T < 1$) and prior old water (1–5 y) to be held in the basin over a longer period of time (Fig. 9).

This finding implies that temperature change plays a key role in drought propagation at snow-dominated basins, because lag response to temperature change varies between wet and dry conditions. An increase up to 8 °C in temperature more than historical conditions leads to little change in the fraction of the wet year's inflow exiting the system in the future five years, but it significantly reduces the fraction of the dry year's inflow leaving the system in both the near future ($T < 1$ y) and over a longer period (1–5 y) (Fig. 9). This means that years with limited precipitation are more sensitive to climate change. In addition, with an increasing fraction of inflow lost to ET, hydrologic connectivity is further decreased and more water remains in the subsurface and becomes old, which propagates droughts in snow-dominated basins even longer.

(Foster et al., 2016) found that with warming, energy budget increases reduced streamflow more than snow-rain transitions. A 4 °C of uniform warming reduced streamflow 44.8% more than a complete shift in precipitation from snow to rain. However, our study showed that large reductions in annual streamflow did not occur until temperature increases exceeded 7 °C. (Fig. S.18). Furthermore, our study showed variations in wet and dry years in terms of streamflow TTD. The transit time decreased with small increases in temperature (2 °C to 4 °C) in dry years, but remained almost the same until temperature increases exceeded 8 °C in wet years, and a significant reduction of TTD only happened with extreme warming (15 °C) when precipitation shifted from snow to rain (Fig. 8a). This finding indicates that energy budget increases in dry years have a greater effect on TTD variations, whereas snow-rain transitions in wet years have a have a greater effect on TTD variations. Furthermore, our study found that more inflow water was flushed from the system in wet years with extreme temperature increases than in dry years under historical conditions, which suggests that the sufficiency of precipitation is a more significant factor in controlling TTDs than energy budget and the type of precipitation.

4.4. Limitation of PRMS-SAS-PEST estimation and related future work

No model can represent the full detail of this large-scale, snow-dominated system. Although the SAS + PEST simulated $\delta^{18}O$ concentration C_Q agreed well with the observations during winter and spring snowmelt, the agreement during the summer monsoon season

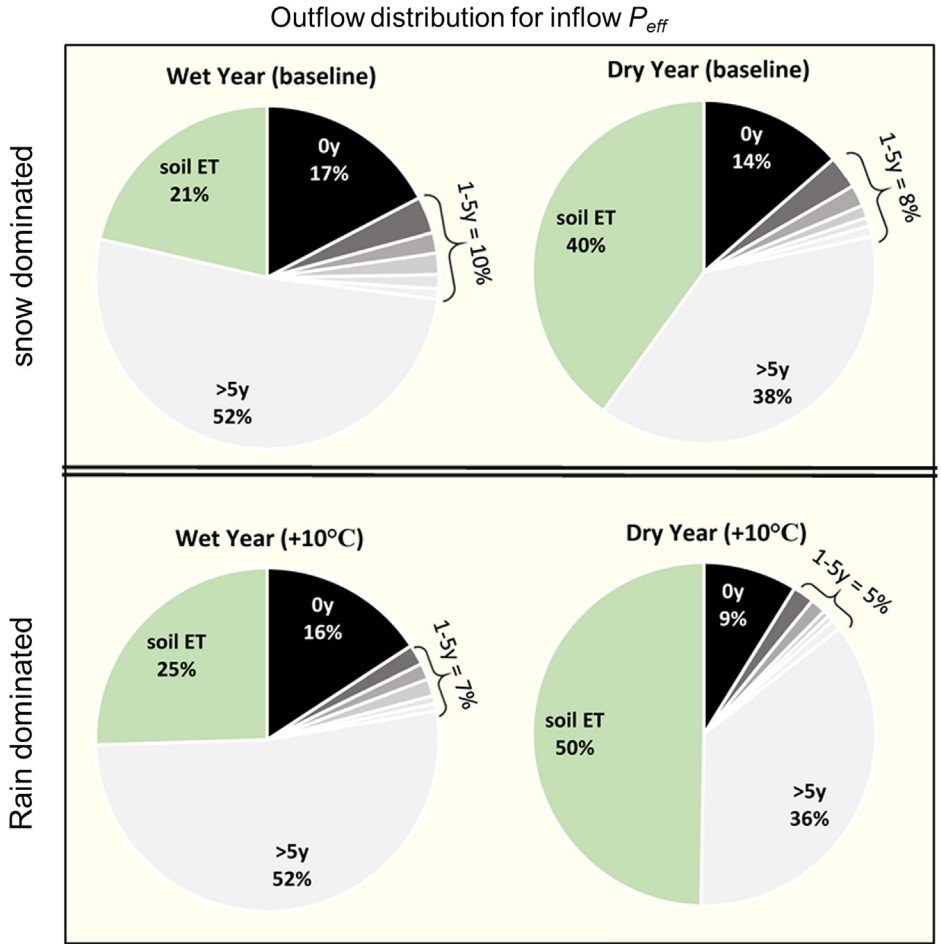

Fig. 9. Lag of representative wet year (left column) and dry year (right column) inflows to exit the basin via stream discharge in the future when temperature increase = 0 °C (i.e., historical conditions) (upper row) and temperature increase = 10 °C (lower row).

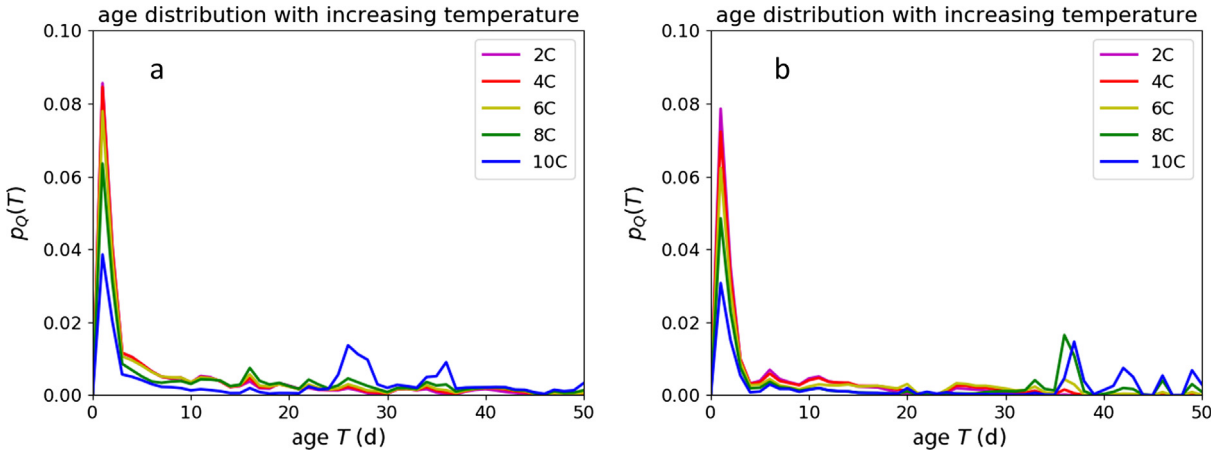

Fig. 10. Simulated age distribution of water under different warming scenarios in years 2011 (a) and 2012 (b).

was poor and highly overestimated (Fig. 5c). (Remondi et al., 2018) found a similar poor agreement and attributed it to the tracer concentration values rapidly shifting toward the concentration of the groundwater storage after a rainfall event. There are also other potential reasons for poor agreement in summer. First, during the summer monsoon season, only the hydraulically connected storage controlled the shape of the SAS function and drove discharge rather than the increasing total storage. A coefficient needed to be added to the total discharge to represent the hydraulically connected storage to better fit the monsoon season. However, it was very difficult to estimate this coefficient with the limited observed $\delta^{18}O$ concentration data, particularly considering this coefficient was heterogeneous depending on the variations of subsurface properties across the catchment. Second, rain during the summer monsoon was largely consumed by *ET*, which greatly affected tracer concentrations of water budget components, but quantifying the uncertainty of *ET* was very difficult (McDonnell et al., 2010). Without direct measured *ET* or C_{ET}, we had to use simulated *ET* and rely on a simple uniform distribution for *ET* in the SAS model.

Subsequently, the strong consumption of rain by *ET* in the summer may not have been well represented by the model, leading to high uncertainty. An introduction of *ET* transit time distribution will help improve the estimates of streamflow TTD. Third, high uncertainty in summer precipitation measurements was reported in recent mountain watershed studies (Hrachowitz and Weiler, 2011) (Daly et al., 2017). Our limited C_J observation during strong summer rain event along with the PRMS estimated rain rate could have also introduced high uncertainty in the SAS model results.

Further limitations arose from assuming uniform precipitation, land surface cover, topography, and soil hydraulic properties in this study. Therefore, the spatial variations of temperature, *SWE*, snowmelt rate and P_{eff}, vegetation and root distribution, elevation and slope, subsurface permeability, soil moisture content, and flow paths on the seasonal and annual dynamics of TTDs were not investigated. However, these factors may play key roles in controlling hydrologic connectivity, water budget, stream discharge, and evapotranspiration variations considering the complicated climate, ecological, and terrestrial structure in snow-dominated systems. For example, spatial patterns of snowmelt are largely determined by the distribution of *SWE* at the start of the melt season (Anderton et al., 2004). Northeast facing slopes receive greater snowmelt inflow than southwest facing slopes during the spring at mountain basins (Kormos et al., 2014). Runoff and *ET* at different elevations have various sensitivities in response to warming (Gilbert and Maxwell, 2018). Introducing entropy in the standard deviation of slope effectively reduces the local hydraulic gradients loss due to spatial aggregation (Fang et al., 2016). As vegetation density increases, hydrologic connectivity decreases at hillslopes with high irradiance but increases at hillslopes with low irradiance (Emanuel et al., 2014). Snowmelt contributions to stream response to summer temperature changes is buffered at higher watersheds than lower watersheds (Lisi et al., 2015). Variations in soil saturation also significantly affect SAS functions. For example, saturated groundwater tends to release younger water to the discharge, whereas the vadose zone prefers older water. Additionally, the influence of recharge rate on the TTD estimation is closely dependent on the heterogeneity of subsurface hydraulic conductivity (Danesh-Yazdi et al., 2018). A lack of representation of three-dimensional heterogeneity in climate, vegetation, topography, and subsurface properties may have hampered the TTD estimates in our PRMS-SAS-PEST model results. Therefore, high resolution three-dimensional climate and hydrologic models such as GSFLOW (Markstrom et al., 2008), PFLOTRAN (Hammond et al., 2014), and ParFlow-CLM (Maxwell and Miller, 2005) will be required to better understand the effect of spatiotemporal distribution variations of climate, surface, and subsurface parameters and quantify the hydrologic response in the future work. Uncertainty quantification of the impacts of climate change on snowmelt-streamflow processes are also important to better understand streamflow TTD response to energy and water budget changes (Kudo et al., 2017).

5. Conclusions

In this study, we coupled PRMS-SAS-PEST models to estimate water budget components, simulate streamflow TTDs, and seasonal and yearly responses to hydrologic and climate changes at a high-altitude snow-dominated watershed in the East River basin. The major findings of this study were:

i. Change in PRMS-estimated water budget components was primarily restricted to dry years with insufficient P_{eff} input when temperature increased.
ii. The inverse storage effect occurred in snow-dominated systems between pre-melt and spring snowmelt seasons, as well as between wet and dry years. Seasonally, more young water was released from storage during spring snowmelt season than winter pre-melt season. Annually, wet years with high P_{eff} contributed more young water in the stream discharge than dry years with water limitations.
iii. Dry year hydrology was more sensitive to climate change than wet year hydrology. An increase of up to 10 °C in temperature over the historical conditions led to little change in the fraction of the wet year's inflow exiting the system five years in the future, but it significantly reduced the fraction of dry year inflow leaving the system for both young water ($T < 1$ y) and old water (1–5 y). With increasing temperature, deep subsurface water was immobilized in dry years and an increasing fraction of inflow was lost to evapotranspiration, which caused hydrologic connectivity to decrease further and more water to remain in the watershed, propagating droughts in snow-dominated basins.
iv. Energy budget increases had a greater effect on TTD variations in dry years, whereas snow-rain transitions had a greater effect TTD variations in wet years. Furthermore, the sufficiency of precipitation was a more significant factor in controlling TTDs than energy budget or the type of precipitation at this snow-dominated watershed.

Declaration of interests

None.

Acknowledgements

Work was supported by the United States Geological Survey through the National Institute of Water Resources under Grant/Cooperative Agreement No. (G16AP00196), and the Lawrence Berkeley National Laboratory's WFSFA through the U.S. Department of Energy Office of Science, Office of Biological and Environmental Research under contract DE-AC02-05CH11231. Special thanks to Wendy Brown for data collection efforts and Markus Bill at LBNL for analytical support.

Appendix A. Supplementary data

Supplementary data to this article can be found online at https://doi.org/10.1016/j.jhydrol.2019.01.029.

References

Allen, S.T., Kirchner, J.W., Goldsmith, G.R., 2018. Predicting Spatial Patterns in Precipitation Isotope (δ2H and δ18O) Seasonality Using Sinusoidal Isoscapes. Geophys. Res. Lett. 45, 4859–4868. https://doi.org/10.1029/2018GL077458.
Anderton, S.P., White, S.M., Alvera, B., 2004. Evaluation of spatial variability in snow water equivalent for a high mountain catchment. Hydrol. Process. 18, 435–453. https://doi.org/10.1002/hyp.1319.
Bales, R.C., Molotch, N.P., Painter, T.H., Dettinger, M.D., Rice, R., Dozier, J., 2006. Mountain hydrology of the western United States. Water Resour. Res. 42, 1–13. https://doi.org/10.1029/2005WR004387.
Barnett, T.P., Adam, J.C., Lettenmaier, D.P., 2005. Potential impacts of a warming climate on water availability in snow-dominated regions. Nature 438, 303–309. https://doi.org/10.1038/nature04141.
Battaglin, W., Hay, L., Markstrom, S., 2011. Simulating the potential effects of climate change in two Colorado basins and at two Colorado ski areas. Earth Interact. 15, 1–23. https://doi.org/10.1175/2011EI373.1.
Benettin, P., Soulsby, C., Birkel, C., Tetzlaff, D., Botter, G., Rinaldo, A., 2017. Using SAS functions and high-resolution isotope data to unravel travel time distributions in headwater catchments. Water Resour. Res. 53, 1864–1878. https://doi.org/10.1002/2016WR020117.
Bhatti, A.M., Koike, T., Shrestha, M., 2016. Climate change impact assessment on mountain snow hydrology by water and energy budget-based distributed hydrological model. J. Hydrol. 543, 523–541. https://doi.org/10.1016/j.jhydrol.2016.10.025.
Botter, G., 2012. Catchment mixing processes and travel time distributions. Water Resour. Res. 48. https://doi.org/10.1029/2011WR011160.
Botter, G., Bertuzzo, E., Rinaldo, A., 2011. Catchment residence and travel time distributions: the master equation. Geophys. Res. Lett. 38. https://doi.org/10.1029/2011GL047666.
Brooks, P.D., Williams, M.W., Schmidt, S.K., 1998. Inorganic nitrogen and microbial biomass dynamics before and during spring snowmelt. Biogeochemistry 43, 1–15. https://doi.org/10.1023/A:1005947511910.
Carroll, R.W.H., Bearup, L.A., Brown, W., Dong, W., Bill, M., Willlams, K.H., 2018. Factors controlling seasonal groundwater and solute flux from snow-dominated basins.

Hydrol. Process. 32, 2187–2202. https://doi.org/10.1002/hyp.13151.
Casper, M.C., Volkmann, H.N., Waldenmeyer, G., Plate, E.J., 2003. The separation of flow pathways in a sandstone catchment of the Northern Black Forest using DOC and a nested Approach. Hydrol. Process. Distrib. Hydrol. Model. 28, 269–275.
Daly, C., Halbleib, M., Smith, J.I., Gibson, W.P., Doggett, M.K., Taylor, G.H., Curtis, J., Pasteris, P.P., 2008. Physiographically sensitive mapping of climatological temperature and precipitation across the conterminous United States. Int. J. Climatol. 28, 2031–2064. https://doi.org/10.1002/joc.1688.
Daly, C., Slater, M.E., Roberti, J.A., Laseter, S.H., Swift, L.W., 2017. High-resolution precipitation mapping in a mountainous watershed: ground truth for evaluating uncertainty in a national precipitation dataset. Int. J. Climatol. 37, 124–137. https://doi.org/10.1002/joc.4986.
Danesh-Yazdi, M., Klaus, J., Condon, L.E., Maxwell, R.M., 2018. Bridging the gap between numerical solutions of travel time distributions and analytical storage selection functions. Hydrol. Process. 32, 1063–1076. https://doi.org/10.1002/hyp.11481.
Diffenbaugh, N.S., Scherer, M., Ashfaq, M., 2013. Response of snow-dependent hydrologic extremes to continued global warming. Nat. Clim. Chang. 3, 379–384. https://doi.org/10.1038/nclimate1732.
Doherty, J., 2015. Calibration and Uncertainty Analysis for Complex Environmental Models. Watermark Numerical Computing, Brisbane, Australia.
Emanuel, R.E., Hazen, A.G., Mcglynn, B.L., Jencso, K.G., 2014. Vegetation and topographic influences on the connectivity of shallow groundwater between hillslopes and streams. Ecohydrology 7, 887–895. https://doi.org/10.1002/eco.1409.
Fang, Z., Bogena, H., Kollet, S., Vereecken, H., 2016. Scale dependent parameterization of soil hydraulic conductivity in 3D simulation of hydrological processes in a forested headwater catchment. J. Hydrol. 536. https://doi.org/10.1016/j.jhydrol.2016.03.020.
Finlay, J., Neff, J., Zimov, S., Davydova, A., Davydov, S., 2006. Snowmelt dominance of dissolved organic carbon in high-latitute watersheds: Implications for characterization and flux of river DOC. Geophys. Res. Lett. 33. https://doi.org/10.1029/2006GL025754.
Flerchinger, G.N., Hanson, C.L., Wight, J.R., 1996. Modeling evapotranspiration and surface energy budgets. Water Resour. Res. 32, 2539–2548.
Foster, L.M., Bearup, L.A., Molotch, N.P., Brooks, P.D., Maxwell, R.D., 2016. Energy budget increases reduce mean streamflow more than snow-rain transitions: Using integrated modeling to isolate climate change impacts on Rocky Mountain hydrology. Environ. Res. Lett. 11, 44015. https://doi.org/10.1088/1748-9326/11/4/044015.
Gaskill, D.L., Mutschler, F.E., Kramer, J.H., Thomas, J.A., Zahony, S.G., 1991. Geologic map of the Gothic Quadrangle. Gunnison County, Colorado.
Gilbert, J.M., Maxwell, R.M., 2018. Contrasting warming and drought in snowmelt-dominated agricultural basins: revealing the role of elevation gradients in regional response to temperature change. Environ. Res. Lett. 13, 74023. https://doi.org/10.1088/1748-9326/aacb38.
Gustafson, J.R., Brooks, P.D., Molotch, N.P., Veatch, W.C., 2010. Estimating snow sublimation using natural chemical and isotopic tracers across a gradient of solar radiation. Water Resour. Res. 46, 1–14. https://doi.org/10.1029/2009WR009060.
Hammond, G.E., Lichtner, P.C., Mills, R.T., 2014. Evaluating the performance of parallel subsurface simulators: an illustrative example with PFLOTRAN. Water Resour. Res. 50, 208–228. https://doi.org/10.1002/2012WR013483.
Harman, C.J., 2015. Time-variable transit time distributions and transport: theory and application to storage-dependent transport of chloride in a watershed. Water Resour. Res. 51, 1–30. https://doi.org/10.1002/2014WR015707.
Heidbüchel, I., Troch, P.A., Lyon, S.W., Weiler, M., 2012. The master transit time distribution of variable flow systems. Water Resour. Res. 48. https://doi.org/10.1029/2011WR011293.
Hrachowitz, M., Weiler, M., 2011. Uncertainty of precipitation estimates caused by sparse gauging networks in a small, mountainous watershed. J. Hydrol. Eng. 16, 460–471. https://doi.org/10.1061/(ASCE)HE.1943-5584.0000331.
Jacobs, J., 2011. Sustainability of water resources in the colorado river basin. Bridg. Link. Eng. Soc. 41, 6–12.
Kirchner, J.W., Feng, X., Neal, C., 2000. Fractal stream chemistry and its implications for contaminant transport in catchments. Nature 403, 524–527. https://doi.org/10.1038/35000537.
Kirchner, J.W., 2019. Quantifying new water fractions and transit time distributions using ensemble hydrograph separation: theory and benchmark tests. Hydrol. Earth Syst. Sci. 23, 303–349.
Klaus, J., McDonnell, J.J., 2013. Hydrograph separation using stable isotopes: review and evaluation. J. Hydrol. 505, 47–64.
Kormos, P.R., Marks, D., McNamara, J.P., Marshall, H.P., Winstral, A., Flores, A.N., 2014. Snow distribution, melt and surface water inputs to the soil in the mountain rain-snow transition zone. J. Hydrol. 519, 190–204. https://doi.org/10.1016/j.jhydrol.2014.06.051.
Kudo, R., Yoshida, T., Masumoto, T., 2017. Uncertainty analysis of impacts of climate change on snow processes: case study of interactions of GCM uncertainty and an impact model. J. Hydrol. 548, 196–207. https://doi.org/10.1016/j.jhydrol.2017.03.007.
Laudon, H., Seibert, J., Köhler, S., Bishop, K., 2004. Hydrological flow paths during snowmelt: congruence between hydrometric measurements and oxygen 18 in meltwater, soil water, and runoff. Water Resour. Res. 40. https://doi.org/10.1029/2003WR002455.
Lisi, P.J., Schindler, D.E., Cline, T.J., Scheuerell, M.D., Walsh, P.B., 2015. Watershed geomorphology and snowmelt control stream thermal sensitivity to air temperature. Geophys. Res. Lett. 42, 3380–3388. https://doi.org/10.1002/2015GL064083.
Longley, P., 2017. Quantifying the Effects of Changing Snowpack Dynamics on Hydrologic Partitioning at Multiple Spatial Scales. ProQuest Diss. Theses.
López-Moreno, J.I., Revuelto, J., Fassnacht, S.R., Azorín-Molina, C., Vicente-Serrano, S.M., Morán-Tejeda, E., Sexstone, G.A, 2014. Snowpack variability across various spatio-temporal resolutions. Hydrol. Process. 1224, 1213–1224. https://doi.org/10.1002/hyp.10245.
Markstrom, S.L., Hay, L.E., Ward-Garrison, C.D., Risley, J.C., Battaglin, W.A, Bjerklie, D.M., Chase, K.J., Christiansen, D.E., Dudley, R.W., Hunt, R.J., Koczot, K.M., Mastin, M.C., Regan, R.S., Viger, R.J., Vining, K.C., Walker, J.F., 2012. Integrated watershed-scale response to climate change for selected basins across the United States. U.S. Geological Survey Scientific Investigations Report 2011–5077 143.
Markstrom, S.L., Niswonger, R.G., Regan, R.S., Prudic, D.E., Barlow, P.M., 2008. GSFLOW—Coupled Ground-Water and Surface-Water Flow Model Based on the Integration of the Precipitation-Runoff Modeling System (PRMS) and the Modular Ground-Water Flow Model (MODFLOW-2005), U.S. Geological Survey. doi:10.13140/2.1.2741.9202.
Markstrom, S.L., Regan, R.S., Hay, L.E., Viger, R.J., Webb, R.M.T., Payn, R.A., LaFontaine, J.H., 2015. PRMS-IV, the Precipitation-Runoff Modeling System , Version 4. U.S. Geol. Surv. Tech. Methods, B. 6 Model. Tech. chap. B7 158, doi: 10.3133/tm6B7.
Maxwell, R., Miller, N.L., 2005. Development of a Coupled Land Surface and Groundwater Model. J. Hydrometeorol. 6, 233–247. https://doi.org/10.1175/JHM422.1.
Maxwell, R.M., 2013. A terrain-following grid transform and preconditioner for parallel, large-scale, integrated hydrologic modeling. Adv. Water Resour. 53, 109–117. https://doi.org/10.1016/j.advwatres.2012.10.001.
McDonnell, J.J., McGuire, K., Aggarwal, P., Beven, K.J., Biondi, D., Destouni, G., Dunn, S., James, A., Kirchner, J., Kraft, P., Lyon, S., Maloszewski, P., Newman, B., Pfister, L., Rinaldo, A., Rodhe, A., Sayama, T., Seibert, J., Solomon, K., Soulsby, C., Stewart, M., Tetzlaff, D., Tobin, C., Troch, P., Weiler, M., Western, A., Wörman, A., Wrede, S., 2010. How old is streamwater? Open questions in catchment transit time conceptualization, modelling and analysis. Hydrol. Process. https://doi.org/10.1002/hyp.7796.
McGuire, K.J., McDonnell, J.J., 2006. A review and evaluation of catchment transit time modeling. J. Hydrol. 330, 543–563. https://doi.org/10.1016/j.jhydrol.2006.04.020.
Molotch, N.P., Brooks, P.D., Burns, S.P., Litvak, M., Monson, R.K., McConnell, J.R., Musselman, K., 2009. Ecohydrological controls on snowmelt partitioning in mixed-conifer sub-alpine forests. Ecohydrology 2, 129–142. https://doi.org/10.1002/eco.48.
Payn, R.A., Gooseff, M.N., Benson, D.A., Cirpka, O.A., Zarnetske, J.P., Bowden, W.B., McNamara, J.P., Bradford, J.H., 2008. Comparison of instantaneous and constant-rate stream tracer experiments through non-parametric analysis of residence time distributions. Water Resour. Res. 44. https://doi.org/10.1029/2007WR006274.
Remondi, F., Kirchner, J.W., Burlando, P., Fatichi, S., 2018. Water Flux tracking with a distributed hydrological model to quantify controls on the spatiotemporal variability of transit time distributions. Water Resour. Res. 54, 3081–3099. https://doi.org/10.1002/2017WR021689.
Rinaldo, A., Benettin, P., Harman, C.J., Hrachowitz, M., McGuire, K.J., Van Der Velde, Y., Bertuzzo, E., Botter, G., 2015. Storage selection functions: A coherent framework for quantifying how catchments store and release water and solutes. Water Resour. Res. https://doi.org/10.1002/2015WR017273.
Ryan, K.C., Opperman, T.S., 2013. LANDFIRE – A national vegetation/fuels data base for use in fuels treatment, restoration, and suppression planning. For. Ecol. Manage. 294, 208–216. https://doi.org/10.1016/j.foreco.2012.11.003.
Sanford, W.E., Pope, J.P., 2013. Quantifying groundwater's role in delaying improvements to Chesapeake Bay water quality. Environ. Sci. Technol. 47, 13330–13338. https://doi.org/10.1021/es401334k.
Siderius, C., Biemans, H., Wiltshire, A., Rao, S., Franssen, W.H.P., Kumar, P., Gosain, A.K., van Vliet, M.T.H., Collins, D.N., 2013. Snowmelt contributions to discharge of the Ganges. Sci. Total Environ. 468–469. https://doi.org/10.1016/j.scitotenv.2013.05.084.
Stockinger, M.P., Lücke, A., Vereecken, H., Bogena, H.R., 2017. Accounting for seasonal isotopic patterns of forest canopy intercepted precipitation in streamflow modeling. J. Hydrol. 555, 31–40. https://doi.org/10.1016/j.jhydrol.2017.10.003.
Stone, R.S., Dutton, E.G., Harris, J.M., Longenecker, D., 2002. Earlier spring snowmelt in northern Alaska as an indicator of climate change. J. Geophys. Res. Atmos. 107. https://doi.org/10.1029/2000JD000286.
Taylor, S., Feng, X., Kirchner, J.W., Osterhuber, R., Klaue, B., Renshaw, C.E., 2001. Isotopic evolution of a seasonal snowpack and its melt. Water Resour. Res. 37, 759–769. https://doi.org/10.1029/2000WR900341.
van der Velde, Y., Heidbüchel, I., Lyon, S.W., Nyberg, L., Rodhe, A., Bishop, K., Troch, P.A., 2015. Consequences of mixing assumptions for time-variable travel time distributions. Hydrol. Process. 29, 3460–3474. https://doi.org/10.1002/hyp.10372.
Van Der Velde, Y., Torfs, P.J.J.F., Van Der Zee, S.E.A.T.M., Uijlenhoet, R., 2012. Quantifying catchment-scale mixing and its effect on time-varying travel time distributions. Water Resour. Res. 48. https://doi.org/10.1029/2011WR011310.
Vivoni, E.R., Rodríguez, J.C., Watts, C.J., 2010. On the spatiotemporal variability of soil moisture and evapotranspiration in a mountainous basin within the North American monsoon region. Water Resour. Res. 46. https://doi.org/10.1029/2009WR008240.
Webb, R.W., Fassnacht, S.R., Gooseff, M.N., 2018. Hydrologic flow path development varies by aspect during spring snowmelt in complex subalpine terrain. Cryosphere 12, 287–300. https://doi.org/10.5194/tc-12-287-2018.
Wilusz, D.C., Harman, C.J., Ball, W.P., 2017. Sensitivity of catchment transit times to rainfall variability under present and future climates. Water Resour. Res. 53, 10231–10256. https://doi.org/10.1002/2017WR020894.
Winnick, M.J., Carroll, R.W.H., Williams, K.H., Maxwell, R.M., Dong, W., Maher, K., 2017. Snowmelt controls on concentration-discharge relationships and the balance of oxidative and acid-base weathering fluxes in an alpine catchment, East River. Colorado. Water Resour. Res. 53, 2507–2523. https://doi.org/10.1002/2016WR019724.

Yang, J., Chu, X., 2013. Quantification of the spatio-temporal variations in hydrologic connectivity of small-scale topographic surfaces under various rainfall conditions. J. Hydrol. 505, 65–77. https://doi.org/10.1016/j.jhydrol.2013.09.013.

Zhai, R., Tao, F., Xu, Z., 2017. Spatial-temporal changes in river runoff and terrestrial ecosystem water retention under 1.5 °C and 2 °C warming scenarios across. China. Earth Syst. Dyn. Discuss 1–31. https://doi.org/10.5194/esd-2017-96.